International Journal of Pharmaceutics 653 (2024) 123876

Contents lists available at ScienceDirect

International Journal of Pharmaceutics

journal homepage: www.elsevier.com/locate/ijpharm

Hypericin emulsomes combined with hollow microneedles as a non-invasive photodynamic platform for rheumatoid arthritis treatment

Heba Abd-El-Azim [a], Haidy Abbas [a,*], Nesrine El Sayed [b], Mohamed R. Mousa [c], Hadil M. Elbardisy [d], Mariam Zewail [a]

[a] Department of Pharmaceutics, Faculty of Pharmacy, Damanhour University, Damanhour, Egypt
[b] Department of Pharmacology and Toxicology, Faculty of Pharmacy, Cairo University, Cairo, Egypt
[c] Department of Pathology, Faculty of Veterinary Medicine, Cairo University, Egypt
[d] Department of Pharmaceutical Analysis, Faculty of Pharmacy, Damanhour University, Damanhour, Egypt

ARTICLE INFO

Keywords:
Microneedles
Photodynamic therapy
Autoimmune diseases
Photosensitizers

ABSTRACT

Rheumatoid arthritis (RA) is a joint-destructive autoimmune disease that severely affects joint function. Despite the variability of treatment protocols, all of them are associated with severe side effects that compromise patient compliance. The main aim of the current study is to prepare localized effective RA treatment with reduced side effects by combining nanoencapsulation, photodynamic therapy (PDT) and hollow microneedles (Ho-MNs) to maximize the pharmacological effects of hypericin (HYP). To attain this, HYP-loaded emulsomes (EMLs) were prepared, characterized and administered through intradermal injection using AdminPen™ Ho-MNs combined with PDT in rats with an adjuvant-induced RA model. The prepared EMLs had a spherical shape and particle size was about 93.46 nm with an absolute entrapment efficiency. Moreover, confocal imaging indicated the interesting capability of Ho-MNs to deposit the HYP EMLs to a depth reaching 1560 μm into the subcutaneous tissue. *In vivo,* study results demonstrated that the group treated with HYP EMLs through Ho-MNs combined with PDT had no significant differences in joint diameter, TNF-α, IL1, HO-1, NRF2 and SD levels compared with the negative control group. Similarly, rats treated with the combination of HYP EMLs, Ho-MNs and PDT showed superior joint healing efficacy compared with the groups treated with HYP EMLs in dark, HYP ointment or HYP in microneedles in histopathological examination. These findings highlight the promising potential of photo-activated HYP EMLs when combined with Ho-MNs technology for RA management. The presented therapeutic EMLs-MNs platform could serve as a powerful game-changer in the development of future localized RA treatments.

1. Introduction

Arthritis, a common term describing joint disorders, refers to joint inflammation associated with pain, swelling and stiffness (Zewail et al., 2021). There are more than 100 types of arthritis, Rheumatoid arthritis (RA) is a chronic autoimmune disorder that is characterized by synovial fibroblast hyperplasia (Aggarwal and Harikumar, 2009), synovial membrane inflammation and pannus formation (Zewail et al., 2021; Firestein, 2003; Farrugia and Baron, 2016).

The exact RA etiology is unknown; however, many genetic and environmental factors are pivotal for its development and progression. (Anita et al., 2021). RA side effects exceed its effect on the joints as it may affect other body organs like the heart and the lungs (Maiuolo et al., 2021; Abbas et al., 2022b).

Several RA treatments include non-steroidal anti-inflammatory drugs, glucocorticoids, disease-modifying anti-rheumatic drugs (DMARDs) and biological agents (Zewail et al., 2021; Yang et al., 2017; Wang and Sun, 2017). Besides the aforementioned RA treatments, photodynamic Therapy (PDT) has become one of the most promising autoimmune disease treatments including RA as it is an easily conducted non-invasive method (Gallardo-Villagrán et al., 2019).

PDT is a medical treatment that uses a photosensitizing agent (PA), a light source, and oxygen to destroy abnormal cells. Once activated by the light irradiation, the agent produces reactive oxygen species (ROS) that destroy nearby diseased cells (Abd-El-Azim et al., 2022). Localized PDT is a targeted minimally invasive procedure that received increased

* Corresponding author.
E-mail addresses: haidy_miu2002@yahoo.com, haidy.abass@pharm.dmu.edu.eg (H. Abbas).

https://doi.org/10.1016/j.ijpharm.2024.123876
Received 26 October 2023; Received in revised form 21 January 2024; Accepted 1 February 2024
Available online 7 February 2024

attention due to several advantages including; a) minimal systemic toxicity, b) higher selectivity with minimized damage to normal cells, c) suitability for a single or an adjuvant therapy and d) overcoming the necessity of avoiding light exposure that is usually required during and after treatment sessions of systemically administered (photo sensitizers) PS which would improve the patient's compliance and quality of life (Abd-El-Azim et al., 2022; Bernal et al., 2015).

Localized PDT has shown an interesting potential for the treatment of RA as the inflamed synovial area represented an ideal PDT target. For instance, a previous study involved injecting aminolevulinic acid (ALA) or verteprofin directly into the joints of patients with RA, and then exposing the joints to a specific type of red light. The results showed that PDT reduced inflammation and improved joint mobility in the patients. (Hendrich et al., 2001).

PDT treatment, regardless of the selected photosensitizer, aims to induce cell death in cells involved in inflammation and hyperplasia in the joint, thus limiting abnormal proliferation of synovial tissue. It is possible to increase the accumulation and retention time of PS in target tissues by encapsulating them in nanogel or nano-particles.

Hypericin (HYP) a polycyclic phenanthroperylenequinone derivative, is a naturally occurring photodynamic agent extracted from Hypericum perforatum. It is one of the most potent photosensitizing agents (Abd-El-Azim et al., 2022). HYP slightly reduces cell proliferation, but its performance improves significantly when it is irradiated at its excitation wavelength (Gallardo-Villagrán et al., 2019). Specifically, in RA, HYP was found to reduce inflammation and oxidative stress in human synovial cells by inhibiting the production of inflammatory cytokines, such as interleukin-6. These findings suggested that HYP could have potential as a natural anti-inflammatory agent in the treatment of RA (Zhang et al., 2018). Unfortunately, HYP suffers from poor aqueous solubility, low skin penetration capabilities and the possibility of inducing liver toxicity in high doses (Abd-El-Azim et al., 2022; Shih et al., 2019). Borghi-Pangoni et al. (Borghi-Pangoni et al., 2017) prepared HYP-loaded poloxamer/carbomer gel in 20 %/0.15 % concentration and that gel achieved appropriate in situ gelation and improved the poor aqueous solubility of HYP to some extend (Borghi-Pangoni et al., 2017). Also, Boiy et al. (Boiy et al., 2007) prepared ten different 10 semisolid vehicles with various physicochemical properties that are used frequently in pharmaceutical compounding and reported that irrespective of the vehicle used, extensive HYP accumulation in the stratum corneum was noted. Furthermore, it was reported that HYP produces insoluble lipophilic ion pairs at physiological pH due to its very hydrophobic nature, resulting in limited photoactivity and inadequate delivery to malignant cells (Youssef et al., 2012). Therefore, these limitations highlight the importance of developing an innovative localized delivery system for improving HYP efficacy against RA while reducing its dose.

Microneedles (MNs) are a rapidly growing drug delivery technology designed as micron-scale patches of arranged needles with pointer sharp tips. MNs are fabricated to be strong and long enough to penetrate the upper skin layers but short enough to avoid nerve sensation (Zhang et al., 2022). Thus, MN technology defeats the challenges of needles' phobia, liver metabolism and GIT adverse effects. Moreover, MNs could provide controlled and sustained release of medications. In addition, MNs guarantee high local drug accumulation (Zhang et al., 2022; Larraneta, 2016). Therefore, MNs could offer additional promising choices for managing RA through delivering a variety of protein therapeutics, small and macromolecules. After skin insertion, MNs open microchannels in the cutaneous tissue to allow the passage of drugs across the dermal layers to the targeted arthritic joint directly (Wang et al., 2022).

Interestingly, hollow microneedles (Ho-MNs) are a type of MN that have a hollow core, allowing for the delivery of high volumes of drugs or biologics (Abd-El-Azim et al., 2022). In addition to the other privileges of MNs, Ho-MNs provide the merit of continuous delivery of larger doses of liquid drug formulations through the subcutaneous layers according to a controlled rate of drug flow (Bushra, 2020). Besides, it is a single-step technique that provides a fast onset of action that, in turn, enhances patient compliance (Waghule et al., 2019). Therefore, Ho-MNs showed great assistance in broadening the delivery feasibility of a variety of therapeutic entities, such as denosumab (Bushra, 2020); HYP-loaded lipid nanocapsules (Abd-El-Azim et al., 2022), vaccines (Arya and Prausnitz, 2016) and insulin (Gupta et al., 2009).

Nanoencapsulation offers several advantages in improving drug delivery of various drugs. Nanocarriers are capable of increasing the bioavailability and prolonging the half-life of poorly water-soluble drugs. They can be also loaded with more than one drug (Feng et al., 2019) along with protecting the encapsulated drugs from the gastric content. In addition, nanoencapsulation can facilitate drug transport and distribution in different tissues (Zewail et al., 2021). Nano-systems are also capable of controlling and extending the drug release period. Furthermore, nanocarrier's surface can be functionalized to target certain cells or tissues and consequently side effects associated with systemic drug administration are minimized (Feng et al., 2019; Prosperi et al., 2017; Zewail et al., 2021).

One of the features of RA is defective angiogenesis, which results in increased capillary permeability and the creation of holes up to 700 nm diameter inside the capillary walls. (Yang et al., 2017). As a result, systemically given nanocarriers can target inflamed joints passively via a mechanism comparable to the enhanced permeation and retention effect (EPR) at the tumor site (Prosperi et al., 2017; Zewail et al., 2019) abbreviated as "(ELVIS)" which refers for extravasation through the leaky vasculature and subsequent inflammatory cell-mediated sequestration that occurs as a result of increased pannus vascular permeability and inflammatory cells activation (Zewail et al., 2021; Yuan et al., 2012).

Barras et al. (Barras et al., 2013) prepared lipid nanocapsules loaded with HYP alone or in combination with protoporphyrin. They discovered that the formed lipid nanocapsule increased in vitro photoactivity while slowing the development of mouse xenograft tumors. But as a result of the inadequate transdermal/intradermal distribution, colloidal carriers had a limited influence on enhancing HYP's dermal penetration, mostly in the superficial skin layers (Barras et al., 2013).

Combing nanoencapsulation along with MNs technology have proven to significantly improve drug pharmacokinetics. Transdermal pharmacokinetic studies of sinomenine (SIN) in mice revealed that the AUC 0–800 min of the skin and blood of the SIN-MN group were 1.43 times and 1.63 times higher than that of the SIN gel group, indicating that SIN-MN has the ability to enhance the drug's transdermal absorption (Weng et al., 2021).

Collectively, the integration of nanoencapsulation with MN technology, in this study, would synergistically potentiate the anti-rheumatic efficacy of the developed system.

The main aim of the current research is to prepare HYP emulsomes (EMLs) and investigate the effect of HYP nanoencapsulation followed by intradermal delivery through Ho-MNs combined with PDT on joint healing in rats with adjuvant-induced arthritis model. To our knowledge, this is the first report on the preparation of HYP-loaded EMLs and their applications for RA management through intradermal injection using hollow MNs.

2. Materials and methods

2.1. Materials

Compritol (Glyceryl dibehenate) and Lipoid S 100 (Phosphatidylcholine, content ≥94.0 %) were provided by Gattefosśe (Saint-Priest, France) and Lipoid AG (Ludwigshafen, Germany), respectively. Cholesterol and complete Freund's adjuvant (CFA) was purchased from Sigma-Aldrich (Steinem, Germany). Hypericin (Isolated from H. perforatum, purity >99 % HPLC) was obtained from Planta Natural Products GmbH, Erlgasse 48, Austria. Commercial hypericin ointment (Bianca Rosa®, PE 0.3 % hypericin) was purchased from Bianca Rosa (Canada).

AdminPen™ metallic hollow microneedles were bought from Nano-BioSciences LLC, USA. The rest of the chemicals and reagents are analytical grade.

2.2. Preparation of blank and hypericin-loaded emulsomes

Preparation of HYP was carried out according to the procedure previously reported by Abbas et al. (Abbas et al., 2022b) using the thin film hydration method but with slight modifications. Compritol, Lipoid S 100 and cholesterol were dissolved in a sufficient amount of dichloromethane in a ratio of (1: 1.2: 0.4) in a beaker that was kept in a water bath adjusted at 80 °C on the magnetic stirrer till complete evaporation of the organic solvent and film formation. The formed film was rehydrated using deionized water and this step was followed by 3 ultrasonication cycles (SonicaR 2200 EP S3, Soltec, Milan, Italy) each one is 3 or 5 min at 60 mA. The formed dispersion was stored in the refrigerator at 4 °C and protected from light until further investigation.

For the preparation of HYP EMLs, Fig. 1A, the HYP amount was first dissolved in a minimum amount of dimethyl sulfoxide and added to the lipid phase. The rest of the preparation procedure was carried out by the same procedure that was used for the preparation of blank EMLs.

2.3. Characterization of blank and hypericin-loaded emulsomes

2.3.1. Particle size and zeta potential measurements

EMLs' particle size, PDI and zeta potential were measured using the Zetasizer Nano ZS (Malvern Instruments, Worcestershire, UK) at 25 °C and 173 °C scattering angle.

2.3.2. Morphological evaluation

The morphology of selected HYP EMLs formulation was evaluated using a transmission electron microscope (TEM) (TEM; JEM-100CX; JEOL, Japan) after staining with uranyl acetate, TEM images were captured at magnifications >10,000x.

2.3.3. Entrapment efficiency determination

Entrapment efficiency (EE%) of HYP-EMLs was evaluated by separating the drug-loaded EMLs from the free drug using ultracentrifugation assisted with ultrafiltration through Amicon® ultracentrifugal filters (100 K MWCO) at 14,000 rpm and 4 °C for 30 min (Abd-El-Azim et al., 2022; Permana et al., 2019). Then, the amount of free HYP in the aqueous phase was determined by HPLC assay at 590 nm, as described in Section 2.5. Following that, the encapsulation efficiency (EE%) was determined according to the following equation:

$$EE\% = \frac{Amount\ of\ added\ drug - Amount\ of\ free\ drug}{Amount\ of\ added\ drug}$$

2.3.4. Stability evaluation

Optimized blank and HYP -EMLs formulations were stored in air-tight amber glass bottles at 4 °C and the stability was monitored over a period of 3 month. Initially, preparations were inspected visually for any physical instability sign, such as precipitation, aggregation or separation. Then, samples were examined for particle size, PDI, zeta potential and EE%.

2.4. Assessment of hollow microneedles-assisted delivery of hypericin-loaded emulsomes

2.4.1. Skin sampling and intradermal injection with AdminPen™ hollow microneedles array

Intact full-thickness human skin was obtained from a male volunteer after abdominal plastic surgery. In brief, subcutaneous fats were removed using surgical scissors. The skin surface was rinsed with a normal saline solution, left to dry, wrapped in aluminium foil and kept at −20 °C until further use. It was reported that human skin could be stored

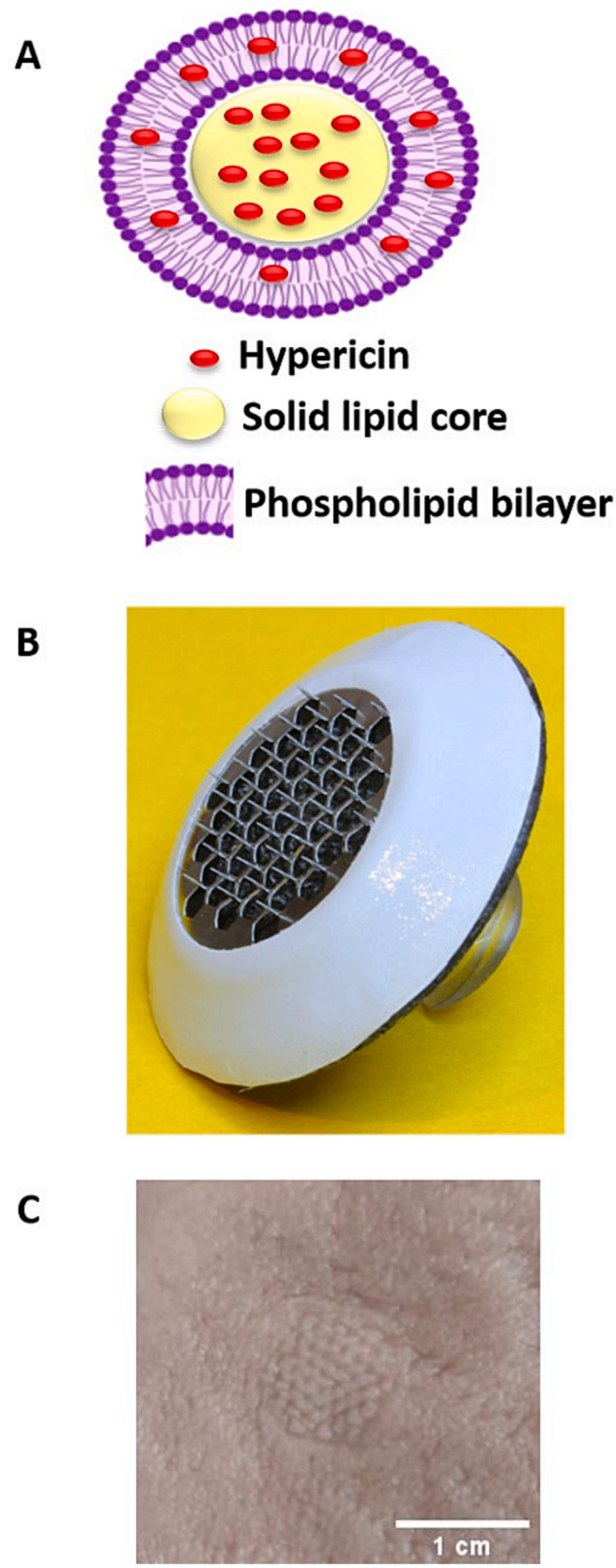

Fig. 1. A) Schematic representation illustrating the prepared HYP EMLs. B) AdminPen™ hollow MNs with 43 stainless-steel MN shafts of 1200 μm in height (Image was used with permission from AdminMed). C) Image captured by a standard mobile camera (Samsung Galaxy Note8, 12 MP, dual pixel, PDAF) showing excised full-thickness human skin after insertion of MNs.

under these conditions for 3–6 months (Dragicevic-Curic et al., 2010).

Both HYP solution and HYP -EMLs were injected into the upper surface of the cleaned full-thickness human skin using AdminPen™, 43 stainless steel metallic Ho-MNs of 1200 μm length located within 1 cm^2 of circular MN array, Fig. 1B. The thumb and the index finger were used to insert the AdminPen™ Ho-MNs into the skin.

2.4.2. Ex vivo insertion features

The skin penetration capabilities of AdminPen™ Ho-MNs were assessed as previously described with some modifications (Abd-El-Azim et al., 2022). The Ho-MNs were inserted into the skin, as stated in Section 2.4.1. Following the removal of Ho-MNs, photographic images were captured for the skin using Samsung Galaxy Note8, 12 MP, dual pixel, PDAF. The number of visible holes created by Ho-MNs was counted and the percentage of percutaneous penetration was also determined according to the following equation:

$$The\ percentage\ of\ penetration = \frac{Number\ of\ created\ holes\ in\ skin}{Total\ number\ of\ hollow\ microneedles} \times 100$$

2.4.3. Ex vivo skin distribution investigation

Ex vivo dermal distribution of free and encapsulated HYP in full-thickness human skin was evaluated using a Leica DMi8 Confocal Laser Scanning Microscope (Leica Microsystems, Wetzlar, Germany). The formulations were intradermally injected using the Ho-MNs and the images were recorded 2 h after treatment.

2.5. Analysis of HYP and construction of the calibration curve

A reversed-phase high-performance liquid chromatographic method (RP-HPLC) previously reported in the literature was followed for HYP analysis (Abd-El-Azim et al., 2022; Wang et al., 2014). The chromatographic system constituted of an Agilent 1290 series (Agilent Technologies, Santa Clara, CA, USA) which was composed of a quaternary pump G4204A, a 100-place auto-injector G4226A, a thermostatted column compartment G1316C controlled at 30 °C and a diode array detector (DAD) G4212A set at a wavelength of 590 nm. This system was linked to a computer with Agilent OpenLAB CDS ChemStation Edition Software installed. Chromatographic separation was conducted on a Microsorb MV-C18 column (250 × 4.6 mm, 5 μm particle size) (Agilent Technologies, the Netherlands). Isocratic elution was applied and the mobile phase was [Methanol: 18.37 mM potassium dihydrogen phosphate (pH 3.5 adjusted using orthophosphoric acid)] 95: 5 %v/v, flowing at a rate of 1.2 mL/min. The injection volume was 20 μL. The run time was 7 min per sample.

The calibration curve was constructed by dilution of HYP standard stock solution with HPLC grade methanol to obtain concentrations within the range of 1–30 μg/ml. Each concentration was injected in thrice into the HPLC system and the average peak areas were computed and plotted against their corresponding concentrations to construct the calibration curve.

2.6. In vivo studies

2.6.1. Ethical statement

The experimental procedures were accepted by the Ethical Committee of the Faculty of Pharmacy, Cairo University, with the permit number (PT 3190). The procedure was performed by the guidelines for the Care and Use of Laboratory Animals (NIH Publication, 2011, 8th Edition).

2.6.2. Experimental animals

Forty adult male Sprague Dawley rats with an average weight of 150 ± 20 g were obtained from the National Centre of Research (Cairo, Egypt), allocated randomly into six groups and housed in the animal facility of the Faculty of Pharmacy, Cairo University. The animals were kept at 25 ± 2 °C and 50 % – 60 % RH on a 12/12 light–dark cycle and had free access to a standard pellet diet, distilled water, and libitum. Before the study, animals were left for one week to acclimatize.

2.6.3. RA induction

Rats were anaesthetized with an intraperitoneal injection of ketamine (50 mg/kg) and xylazine (10 mg/kg). Then, RA induction was carried out on all groups except the negative control. RA induction was performed using an antigen-induced arthritis model (AIA) as previously reported (Zewail et al., 2019; Abbas et al., 2021; Zewail et al., 2021; Zewail et al., 2022). In brief, 200 μL of complete Freund's adjuvant (CFA) was injected in the right knee of each rat, whereas the left knee was kept as control.

2.6.4. Experimental design

Rats were divided into six groups (n = 8), as illustrated in Fig. 2. Group A was kept as the negative control. Group B was left untreated as the positive control group. Treatment started on the third day of the experiment; group C was treated with the daily application of HYP ointment (Bianca Rosa®, St. John's Wort Extract, 0.3 % HYP). Groups D, E and F were treated by intradermal injection using Ho-MNs at days 3 and 10 of the experiment with HYP solution in presence of light, HYP -EMLs in the absence and presence of light, respectively. Irradiation of the arthritic joint only was conducted 45 min after drug administration, using a two-channel Laser Therapy Device, Mustang® 2000+ (Technika Ltd, Russia) at 590 ± 10 nm with a light dose of 150 Jcm^2 and the lamp was adjusted at 5 cm above the platform where rats were placed. HYP dose in both HYP ointment HYP solution and HYP EMLs was equivalent to 0.13 mg/kg (Gallardo-Villagrán et al., 2019; Abd-El-Azim et al., 2022).

After 14 days, rats were anaesthetized and sacrificed by cervical dislocation under anaesthesia with thiopental (50 mg/kg) (Boskabady et al., 2011) and joints were dissected and fixed in 10 % formalin solution. Blood samples were also collected and centrifuged at 5000 rpm at RT for 15 min then the serum was frozen at −80 °C until further analysis.

2.6.5. Joint diameter measurements

Average rat knee joint diameters were assessed during the experiment on days 0, 3, 7 and 14 by utilizing a micrometre (KM-211–101, Shaanxi, China).

2.6.6. Enzyme-linked immunosorbent assay (ELISA)

The serum levels of heme oxygenase (HO-1) (Enzo life sciences, New York, USA), nuclear respiratory factor 2 (NRF2) (Cusabio Technology LL, Houston, USA), tumor necrosis factor-alpha (TNFα), superoxide dismutase (SOD), interleukin 1B (IL1B) (My BioSource, San Deigo, CA, USA), were evaluated using an ELISA kit based on the manufacturer instructions.

2.6.7. Histopathological evaluation

Joints were dissected out and kept in neutral buffered formalin (10 %), After decalcification 20 % EDTA joints were processed in different grades of alcohols, xylene and embedded in paraffin wax. Six μm sections were cut and stained with hematoxylin and eosin (H&E) for light microscopy. Toluidine blue was performed to demonstrate the changes in articular cartilage (Bancroft and Gamble, 2008). Histopathological lesion score was performed as previously illustrated (El-Shiekh et al., 2021). Briefly, histopathological alterations in the joints were evaluated using semiquantitative scoring with five scores (0: unremarkable, 1: minimal, 2: mild, 3: moderate, and 4: marked).

2.7. Statistical analysis

Results were presented as mean ± SD. Statistical analysis of colloidal characteristics of EMLs, joint diameter measurements and ELISA were

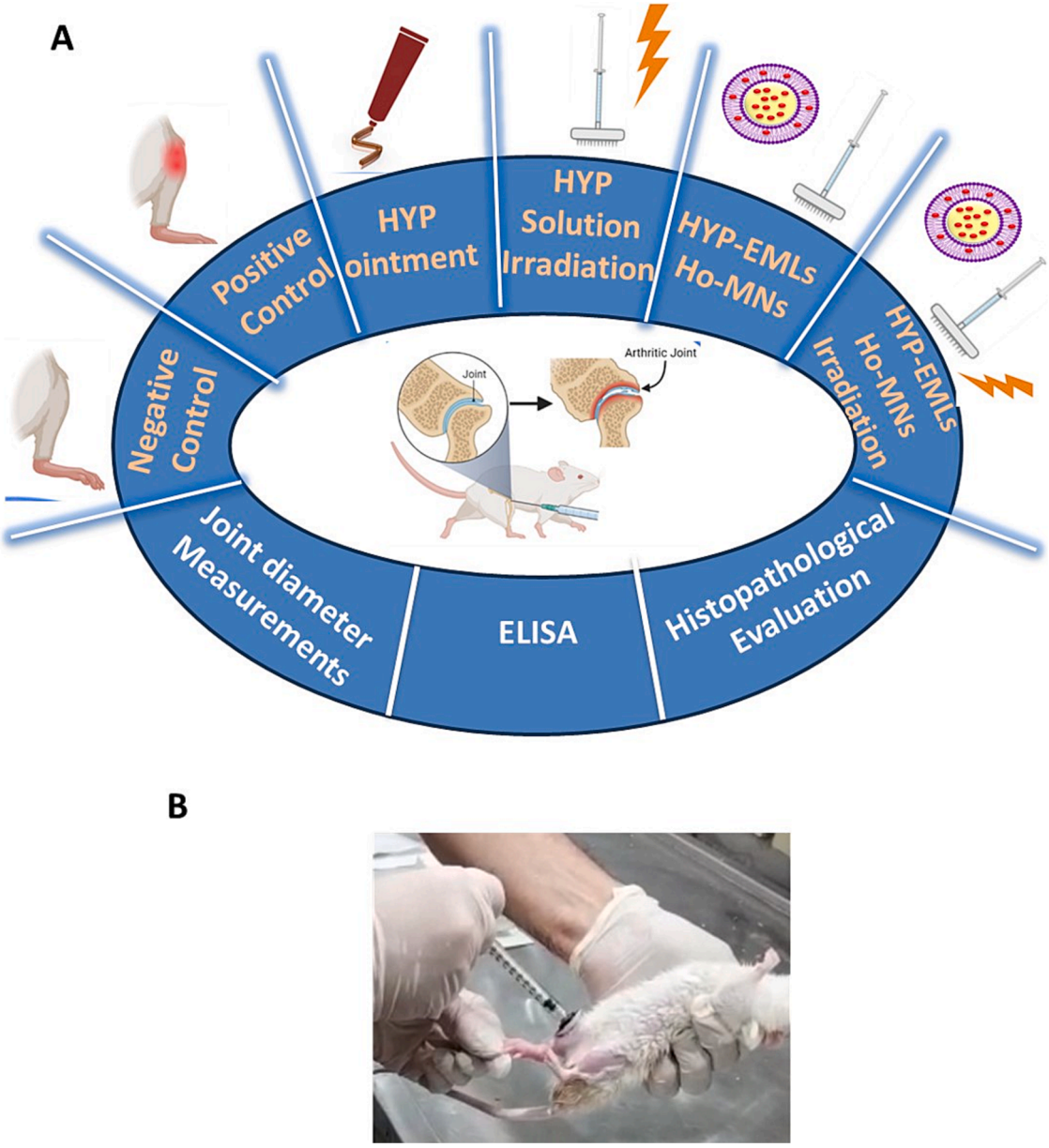

Fig. 2. A) Schematic representation showing the different treatment groups investigated in the *in vivo* study and further characterization techniques. B) Intradermal administration of drug formulations using AdminPen™ hollow MNs into the inflamed rheumatic joint in rats.

conducted by Student's *t*-test ($P < 0.05$), Two-way ANOVA followed by Tukey's test ($P < 0.0001$) and One-way ANOVA followed by Tukey's test ($P < 0.0001$), respectively using Prism 7 software.

3. Results and discussion

3.1. Preparation and evaluation of blank and hypericin-loaded emulsomes

The preparation of EMLs by thin film hydration method was previously reported by Abbas et al. (Abbas et al., 2022b) and Rizk et al. (Rizk et al., 2021). The choice of EMLs was based on their several merits as they are biocompatible nanocarriers that combine the characteristics of emulsions and liposomes as they possess a solid lipid core that is surrounded by phospholipid layers (Kumar and Seth, 2013; Ucisik et al., 2015). The presence of phospholipid bilayer assists in the stabilization of EMLs without surfactant incorporation suggesting their high biocompatibility that enable their diverse applications (Ucisik et al., 2015). Also, EMLs' structure allows the accommodation of higher amounts of drugs compared to liposomes and solid lipid nanoparticles (Kumar, 2010; Zhou and Chen, 2015).Furthermore, EMLs can enhance the solubility of hydrophobic drugs besides their ability to provide a sustained drug release profile. (Bolat et al., 2020).

Besides, lipoid S 100, compritol and cholesterol were included in the formulation of EMLs. The former was chosen due to its hydrophobic nature which would increase the possibility of loading HYP (Paliwal et al., 2009). The latter was added for two reasons. First to increase the stability of the phospholipid layer and the second reason is attributed to the ability of cholesterol to enhance HYP loading into EMLs (Rizk et al., 2021).

3.1.1. Particle size and zeta potential measurements

Different EMLs formulations are listed in Table 1, The effect of homogenization time on the colloidal characteristics of EMLs was investigated. Increasing sonication in the three cycles from 3 min/ cycle to 5 min/cycle resulted in a significant decrease in particle size (student *t*-test

Table 1
HYP concentrations, sonication cycles and colloidal characteristics of HYP EMLs.

Formulation	HYP concentration	Probe sonication	Particle size (nm)	PDI	Zeta potential (meV)
EMLs 1	————	3 min/ cycle (3 cycles) 60 mA	138.0 ± 1.87	0.38 ± 0.04	− 17 ± 0.25
EMLs 2	————	5 min/ cycle (3 cycles)	87.53 ± 1.25	0.19 ± 0.02	− 20.7 ± 0.14
EMLs 3	50 μg/ml	60 mA	93.46 ± 2.77	0.22 ± 0.12	− 21.2 ± 0.34

$P < 0.05$). Particle size decreased from 138 nm to 87.53 nm. This finding is in agreement with the results previously reported by Abbas et al. (Abbas et al., 2022b) and Priyanka et al. (Priyanka et al., 2018). On the other hand, they oppose the results previously reported by Rizk et al (Rizk et al., 2021) who reported that the increase in homogenization time was accompanied by a significant increase in EMLs' particle size. Loading EMLs with HYP resulted in increasing particle size from 87.53 to 93.46 nm.

The particle size is considered one of the most important components influencing the passive targeting approach. This is because nanodrug carriers larger than 200 nm and smaller than 10 nm may be removed by the spleen and kidney, respectively. Thus, only nanodrug carriers with a size of 100–200 nm could resist absorption by the mononuclear phagocyte system and the reticuloendothelial system allowing them to remain in circulation for longer in RA patients (Li et al., 2021), thus the prepared HYP EMLs can provide long circulation half-life ensuring effective uptake by passive targeting mechanism in inflamed rheumatic joints.

All the prepared formulations had PDI values less than 0.4 indicating nanodispersion homogeneity. PDI values reflect the degree of nanodispersion homogeneity, values closer to zero indicate a more uniform dispersion (Mehanna et al., 2020; Zewail et al., 2022). PDI values of the optimized EMLs formulation (EMLs 2 and EMLs 3) are 0.192 and 0.223, respectively indicating the homogeneity of the prepared nanosystem (Abbas et al., 2022a) (Table 1).

As Table 1 illustrates, zeta potential ranged from −17 to −21.2. Loading EMLs with HYP resulted in a slight increase in zeta potential from −20 to −21.2. Zeta potential is a crucial factor in controlling the stability of nanoformulations. High surface charges produce repulsive forces that counteract particle aggregation (Rahman et al., 2013; Zewail et al., 2019; Ahmed et al., 2020). The highest nanocarriers' stability is attained with zeta potential values around ±30 mV therefore the prepared EMLs are considered stable (Abbas et al., 2022a; El-Nabarawi et al., 2020; Abbas et al., 2021).

HYP loaded lipid nanocarriers have been previously reported (Abd-El-Azim et al., 2022; Youssef et al., 2012; Lima et al., 2013). The prepared HYP EMLs in the current study offers higher EE % and smaller particle size compared with HYP solid lipid nanoparticles (SLNs) previously prepared by Lima et al. (Lima et al., 2013) and Youssef et al. (Youssef et al., 2012) The previously prepared HYP SLNs that had EE % of 88.3 % and particle size of 200.33 nm (Youssef et al., 2012).

Also, HYP loaded nanocapsules have been previously reported by Abd-El-Azim et al. (Abd-El-Azim et al., 2022). EMLs are considered superior to nanocapsules as they do not contain surfactants and hence they display no cytotoxic effects (Bolat et al., 2020).

3.1.2. Morphological evaluation

Fig. 3 illustrates that the TEM micrograph showed that HYP -EMLs had uniform spherical shapes with distinct core–shell structures and no signs of aggregation.

3.1.3. Entrapment efficiency determination

The EE% of loaded EMLs were evaluated using the ultracentrifugation-assisted ultrafiltration technique as described in Section 2.3.3 and the amount of unencapsulated HYP was calculated according to the HYP quantitative analysis stated in Section 2.5 using a formerly developed and validated HPLC method (Abd-El-Azim et al., 2022). Six different HYP concentrations namely; 1, 3, 5, 10, 20 and 30 μg/mL were employed for calibration curve construction. Each concentration was injected in triplicate into the chromatographic system and the average peak areas were plotted on the y-axis against their corresponding concentrations on the x-axis. A linear relationship for HYP was observed in the range of 1 – 30 μg/mL and the relevant regression equation was:

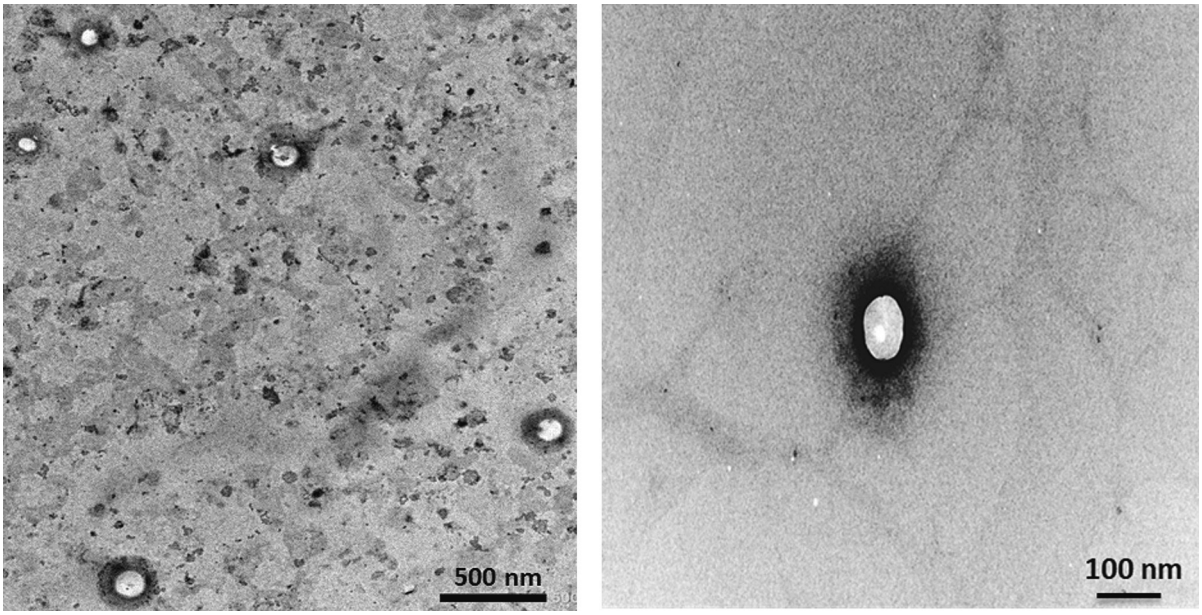

Fig. 3. TEM micrographs of HYP loaded EMLs (EMLs 3) after staining with uranyl acetate with two different magnification powers to illustrate core shell structure of EMLs.

$$Y = -43.76 + 53.83X (R^2 = 0.999)$$

HYP -EMLs 3 yielded an absolute high EE % of 100 % ± 0.02 %. This may be conferred to the effect of EMLs on enhancing the solubility and EE % of hydrophobic drugs (Rizk et al., 2021; Gill et al., 2014) as a result of their structure that incorporates both compritol and cholesterol (Rizk et al., 2021). Besides, comparable EE % values for the hydrophobic HYP were achieved in lipid nanocapsules (Abd-El-Azim et al., 2022; Barras et al., 2013) and solid lipid nanoparticles (Nafee et al., 2013).

3.1.4. Stability evaluation

Upon storage of HYP -EMLs for 3 months at 4 °C, no signs of instability were observed. The optimized formulations maintained their physico-chemical characteristics including homogenous particle size distribution and negative zeta potential, as illustrated in Table 1. Besides, HYP-EMLs kept their EE% values (99 % ± 0.05 %) conferring superior stability without any drug leakage.

3.2. Assessment of hollow microneedles-assisted delivery of hypericin-loaded emulsomes

AdminPen™ Ho-MNs are a cutting-edge advancement in the field of transdermal drug delivery. These MNs are designed to be minimally invasive and offer a highly efficient method of administering liquid medications and vaccines. In this work, AdminPen™ Ho-MNs, 1200 μm, were used to overcome the poor skin permeability of HYP and to enable deeper and localized delivery of HYP-EMLs across the skin layers to the arthritic joint. Each array consists of 43 tiny, hollow, and sharp-tipped stainless-steel structures that can painlessly penetrate the skin's outer layer (Yuzhakov, 2010). The length of these MNs promotes vertical diffusion of the injected formulation, thus allowing for local drug accumulation, resulting in improved localized pharmacological effects (Wang et al., 2022).

The major challenge Ho-MNs encounter is the probability of clogging needle openings when the skin is pierced and thus the flow of the drug is hindered (Waghule et al., 2019). Interestingly, AdminPen™ Ho-MNs arrays are innovatively manufactured with an off-centred hollow pore on its side to avoid needle blockage and to enable continuous efficient drug delivery. When inserted into the skin, AdminPen™ MNs form tiny microchannels in the stratum corneum and epidermis that quickly collapse and thereby the skin barrier is shortly restored after array removal avoiding any risk of developing an infection (Abd-El-Azim et al., 2022; Yuzhakov, 2010). For the aforementioned advantages, AdminPen™ Ho-MNs were chosen to deliver the prepared HYP EMLs deeply across the skin and joint barriers.

3.2.1. Ex vivo insertion features

Successful skin penetration is crucial for MNs to exert their intended action (Permana et al., 2019). With an intent to assess the *ex vivo* insertion potential of the AdminPen™ Ho-MNs, arrays were administered to excised human skin. As shown in Fig. 1C, clear 43 holes were observed after MNs removal indicating that AdminPen™ Ho-MNs successfully and smoothly punctured the stratum corneum recording a dermal penetration percentage of 100 %. Thus, the proposed MN-EMLs combined delivery system revealed a promising potential for the deep transdermal delivery of HYP to arthritic joints.

3.2.2. Ex vivo skin distribution investigation

To achieve the main aim of the current work of delivering HYP EMLs deeply into the arthritic joint through the skin, the loaded EMLs were injected into full-thickness excised human skin using AdminPen™ Ho-MNs where liquid formulations were freely flowed into the deeper skin layers through the created micro-passages without any needle blockage or drug leakage.

Confocal imaging was used to visualize the extent of intradermal distribution of the fluorescent HYP from loaded EMLs versus control drug solution following AdminPen™ Ho-MNs application. Furthermore, the fluorescence signal recorded by confocal microscopy could be correlated to the HYP solubility in biological samples (Abd-El-Azim et al., 2022; Boiy et al., 2007). The generated images, Fig. 4, showed stronger fluorescence intensity in the case of HYP EMLs compared to hardly detected fluorescent signal for free drug solution reflecting higher solubility for encapsulated HYP. Besides, data showed the distribution of HYP EMLs to a depth of 1560 μm within the skin layers relative to only 800 μm for free HYP. The obtained results revealed that HYP EMLs were able to move within the skin layers and distribute themselves to a depth beyond the MN length (1200 μm).

Importantly, these promising observations could be attributed to the hydrophobic nature of the free HYP that leads to the formation of stable non-fluorescent aggregates in biological tissues. These insoluble aggregates strongly interact with the stratum corneum limiting the intradermal distribution of free HYP (Barras et al., 2013). In addition, the tendency of free HYP to form hydrogen bonding with the surrounding biological components represents another factor hindering its skin penetration (Boiy et al., 2007). Interestingly, encapsulation of HYP into EMLs masked its ability to form unwanted hydrogen bonding, prevented aggregate formation and improved its solubility in biological conditions. Thereby, EMLs improved the depth and extent of intradermal distribution for HYP. Collectively, the presented Ho-MN platform combined with EMLs could hypothetically boost the localized delivery of HYP into arthritic joints for enhanced therapeutic outcomes.

3.3. In vivo studies

RA transdermal drug delivery approach is considered a successful alternative to invasive routes that compromise patient compliance. MNs are considered one of commonly used transdermal delivery systems (Balata et al., 2020; Zhang et al., 2022). The drug absorption mechanisms following transdermal administration can be divided into the skin appendage route and the transepidermal route which is considered the main absorption route following transdermal drug delivery. The transepidermal route can be further divided into the transcellular route and intercellular route. The latter is considered the main pathway of drug absorption (Zhang et al., 2022). MNs can cause drugs to directly penetrate the stratum corneum, which helps the drugs to be directly absorbed by the capillaries and lymphoid tissues in the dermis (Zhang et al., 2022).RA induction was carried out by the AIA model. The choice of this model was based on the well-documented results of its ability to effectively induce RA (van Eden et al., 1996; Butler et al., 1992; Liu et al., 2009). CFA which is composed of heat-killed microbacterium tuberclosis was used in AIA induction. The left knee was only injected while the right one was kept as a control. Treatment started on the third day after RA induction. Group C administered HYP ointment at a daily dose of 0.13 mg/kg (Gallardo-Villagrán et al., 2019; Abd-El-Azim et al., 2022), on the other hand, groups D & E were treated with HYP EMLs in the presence and absence of light by administration of two intradermal injections by Ho-MNs at day 3 and 10 of the experiment each loaded with HYP dose of 0.13 mg/kg (Gallardo-Villagrán et al., 2019; Abd-El-Azim et al., 2022).

The selection of HYP dose was based on a previous cell culture study using a melanoma cell line performed by the author, Abd-El-Azim and colleagues (Abd-El-Azim et al., 2022), that tested the cytotoxicity of HYP over a concentration range of 0 to 5 μM and reported a potent cytotoxic effect in a dose dependent manner.

3.3.1. Joint diameter measurements

Average joint diameters were measured on days 0, 3, 7 and 14 days of the experiment (Fig. 5A). The morphological examination of paws and joints in different experimental groups at the end of the experiment is illustrated in Fig. 5B that shows that the group treated with HYP EMLs MNs in the presence of light showed nearly normal joint shape compared with the negative control group. Also, the group treated with HYP EMLs

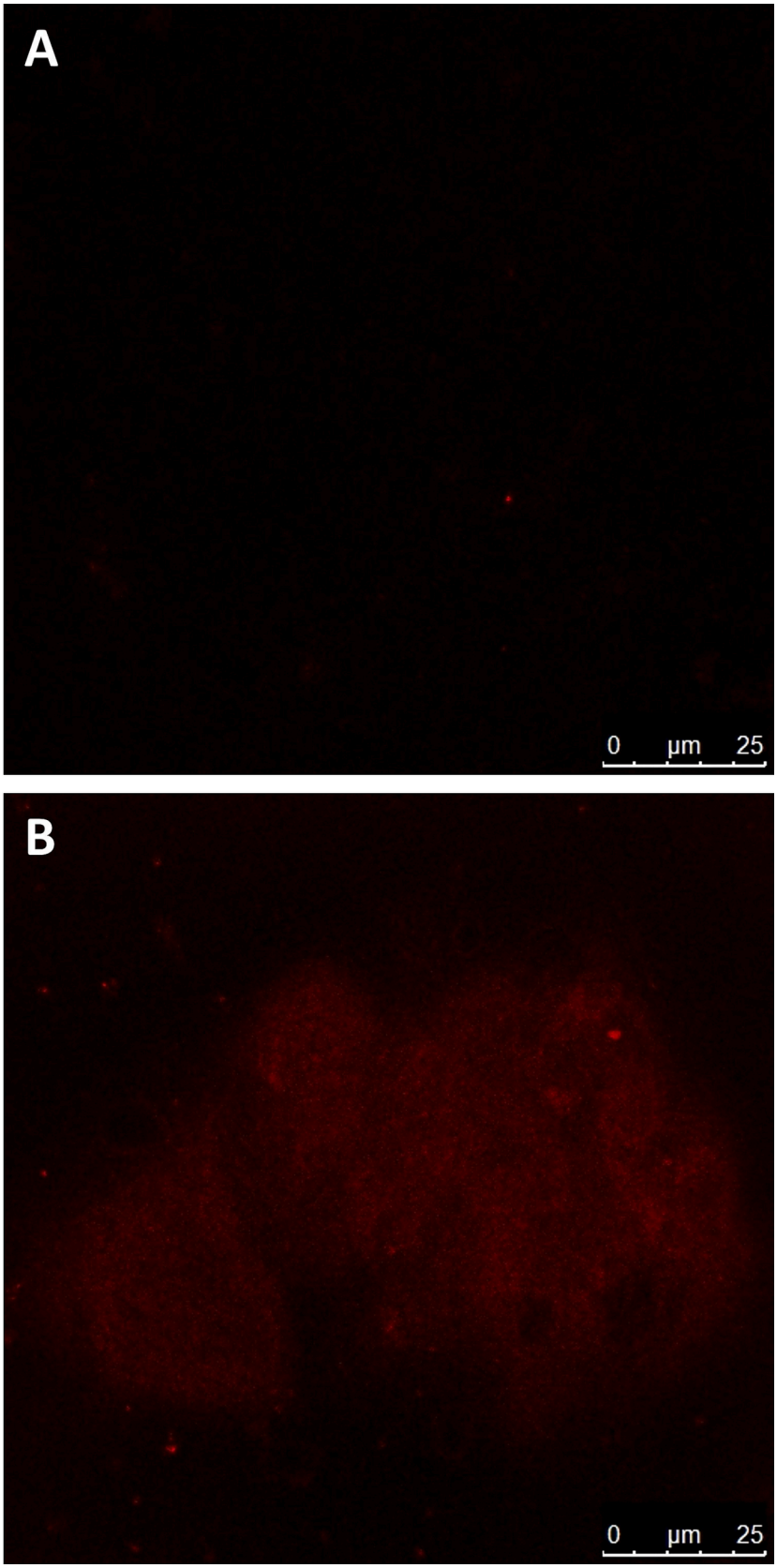

Fig. 4. Confocal fluorescence images of excised full thickness human skin after injection of, A) HYP solution as a control and B) HYP EMLs using AdminPen™1200 µm Ho-MNs.

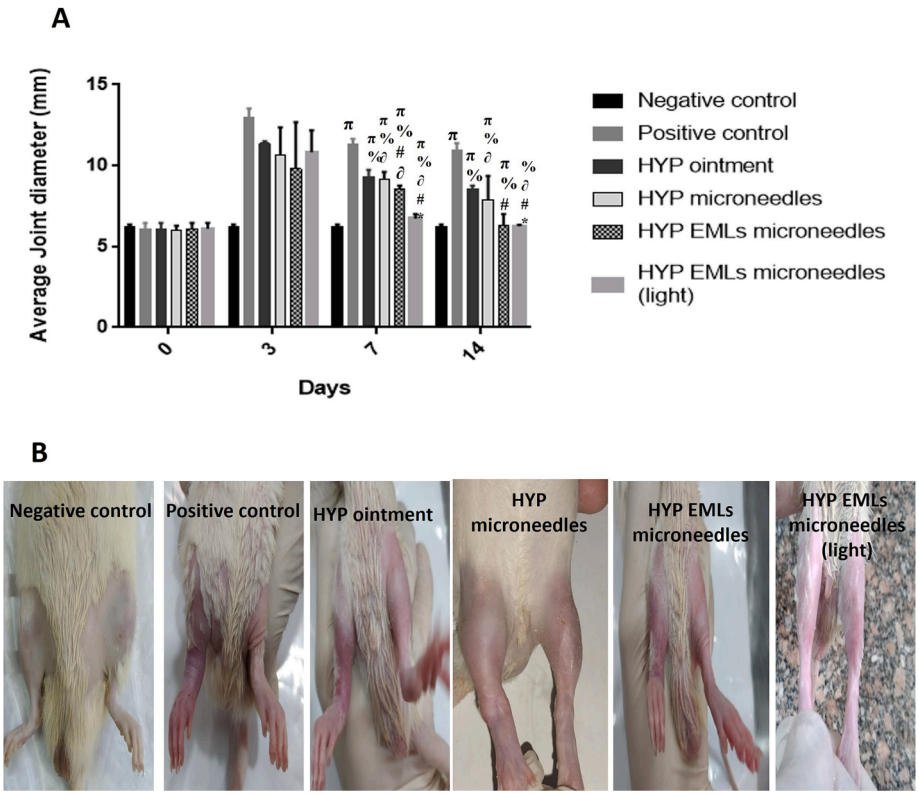

Fig. 5. (A) Average joint diameters of different experimental groups on days 0, 3, 7 and 14. (B) Joint morphology at the end of the experiment.Statistical analysis was carried out using two-way ANOVA followed by Tukey's test. π significant difference from negative control. % significant difference from positive control. * significant difference from HYP EMLs in absence of light. ∂ significant difference from HYP ointment. # significant from HYP microneedles.

MNs in the absence of light showed better joint and paw condition compared with HYP solution in microneedles in presence of light and HYP ointment.

Statistical analysis of joint diameter data revealed that at day 0, no statistically significant differences was noted among the different experimental groups meanwhile at day 3 (after RA induction) statistically significant differences were noted between the negative control group and the rest of the experimental groups. Results at day 14 revealed that all groups showed statistically significant differences from the negative control group except the group treated with HYP EMLs Ho-MNs in the presence of light. Furthermore, all treatment groups demonstrated statistically significant differences among each other and from the positive control group.

3.3.2. ELISA

Several factors contribute to RA progression and invasiveness. Immune modulation is a key player in RA progression in which TNF-α has a leading role (Farrugia and Baron, 2016; Zewail et al., 2021). Stimulation of TNF-α is accompanied by stimulation of different cells like T cells, dendritic cells and B-cells which in turn will lead to T cell activation and differentiation (Farrugia and Baron, 2016). Another inflammatory mediator is IL1B which is significantly elevated in the serum of RA patients compared to osteoarthritis and non-inflammatory joint diseases. Both TNFα and IL1 can trigger the release of matrix metalloproteinases that degrade the cartilage. Also, they can increase the production of proinflammatory genes that will eventually lead to over production of different proinflammatory mediators like nitric oxide and prostaglandin E2 (Kay and Calabrese, 2004). Besides, TNFα and IL1, HO-1 has regulatory roles in the progression of RA inflammation. Another factor that contributes to RA pathogenesis is the reduced NRF2 levels. Both NRF2 and SOD levels are downregulated in RA patients. NRF2 has a direct effect on the production of antioxidant enzymes that protect the cells from damage through free radical production suppression (Chadha et al., 2020b). Also, SOD plays a crucial role in ROS scavenging and eventually inflammation can be alleviated (Srivastava, 2017).

At the end of the experiment levels of TNFα, IL1, HO, SOD, MMP 9 and NRF2 were assessed (Fig. 6). Induction of RA resulted in increasing the levels of TNFα, IL1, HO and MMP 9 while the levels of NRF2 and SOD are reduced. These finding are along with the previous reports (Abbas et al., 2022; Srivastava, 2017; Chadha et al., 2020a; Odobasic et al., 2014; Fernandes et al., 2012). Levels of TNF α were 159.5, 97.2, 59.2, 82.7, 43 and 41.2 pg/ml in the groups for the positive control, groups treated with HYP ointment, HYP in microneedles, HYP EMLs in Ho-MNs in the absence and presence of light and the negative control group, respectively.

Levels of IL1β were elevated by 2.86, 1.545, 1.25 and 1.04 folds in the positive control, groups treated with HYP ointment, HYP in microneedles HYP EMLs in Ho-MNs in the absence and presence of light, respectively. Also, levels of MMP 9 showed 3.59, 2.24, 1.36, 1.47 and 1.14 folds increases in the mediator level compared with the negative control group for the aforementioned groups in the same order.

Levels of HO were elevated by 6.2, 3.3, 3, 2.3 and 1 folds in the positive control, groups treated with HYP ointment, HYP in microneedles and HYP EMLs in Ho-MNs in the absence and presence of light, respectively compared with the negative control group.

On the other hand, NRF2 level was 55.1, 78.9, 83, 96.4, 103 and 105 ng/ml for the positive control, groups treated with HYP ointment, HYP in microneedles, HYP EMLs in Ho-MNs in the absence and presence of light, and the negative control group, respectively.

The present study showed that the levels of the studied inflammatory mediator were statistically significant in all treatment groups compared to the positive control group. There was also a statistically significant difference between the groups treated with HYP ointment, HYP in microneedles and the groups treated with HYP EMLs. In addition, there were statistically significant differences between the groups treated with HYP EMLs in Ho-MNs in the absence and presence of light. All groups

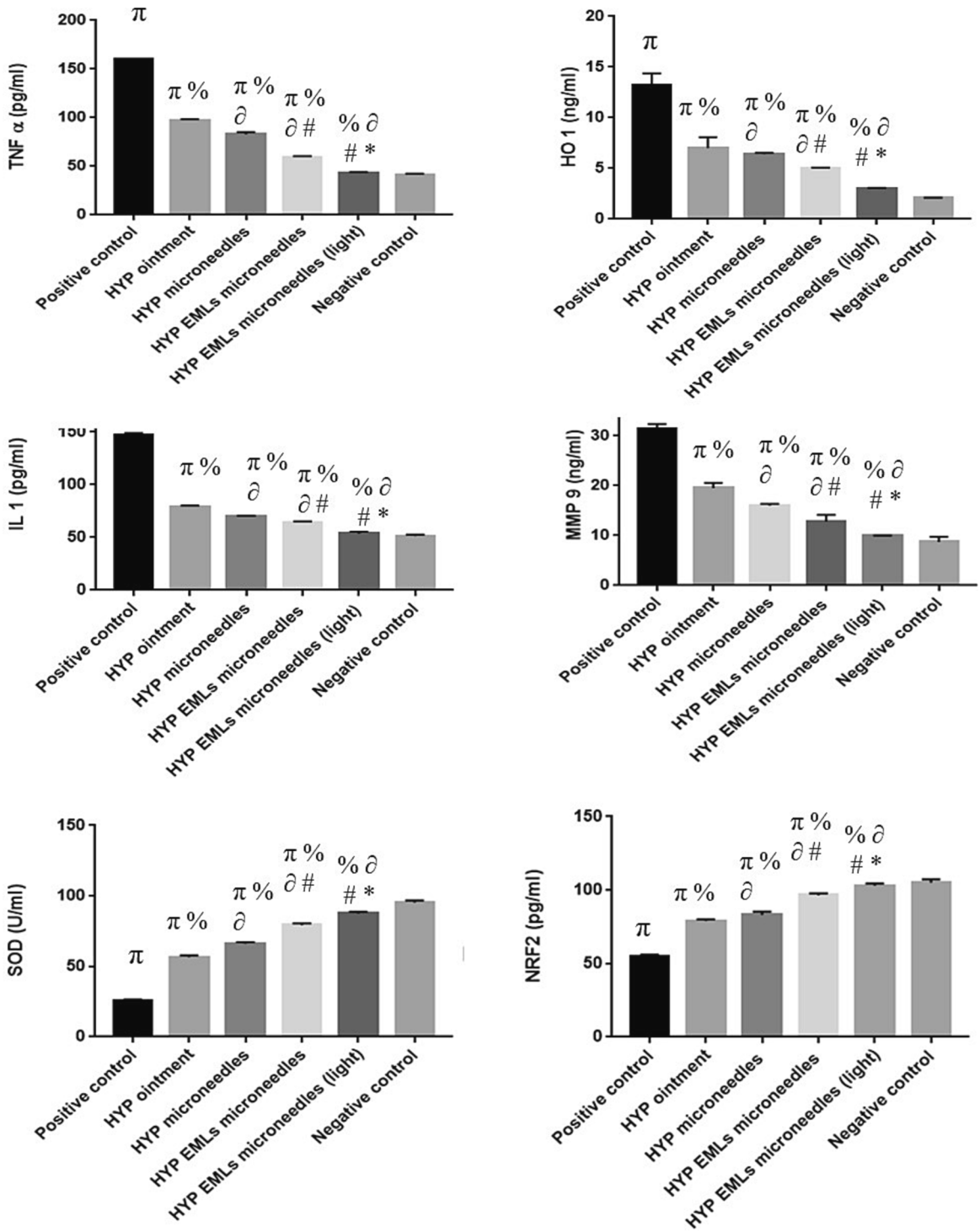

Fig. 6. Serum levels of TNF α, HO, IL1, MMP 9, SOD and NRF2 of different experimental groups at the end of the experiment. Statistical analysis were carried out using one-way ANOVA followed by Tukey's test. π significant difference from negative control. % significant difference from positive control. * significant difference from HYP EMLs in absence of light. ∂ significant difference from HYP ointment. # significant from HYP microneedles.

showed statistically significant differences from the negative control group except the group treated with HYP EMLs in Ho-MNs in the presence of light.

3.3.3. Histopathological evaluation

As shown in Fig. 7, the examined sections of positive control group revealed intense inflammatory cells infiltration around the joint capsule that extended deep into the synovial membrane with marked sloughing of its lining. The articular cartilage suffered from degenerative changes in some chondrocytes. Joints sections from HYP ointment group showed mild improvement as the severity of inflammation was reduced but there were some inflammatory cells infiltrating into the joint capsule. The articular cartilage was apparently normal. Similar results were detected in HYP microneedles. More protective action was noticed in the sections from HYP EMLS microneedles group; periarticular edema was the only detectable alteration with apparently normal synovial membrane and articular cartilage. The best protective effect was exerted by HYP EMLS microneedles (light) as almost all examined sections were

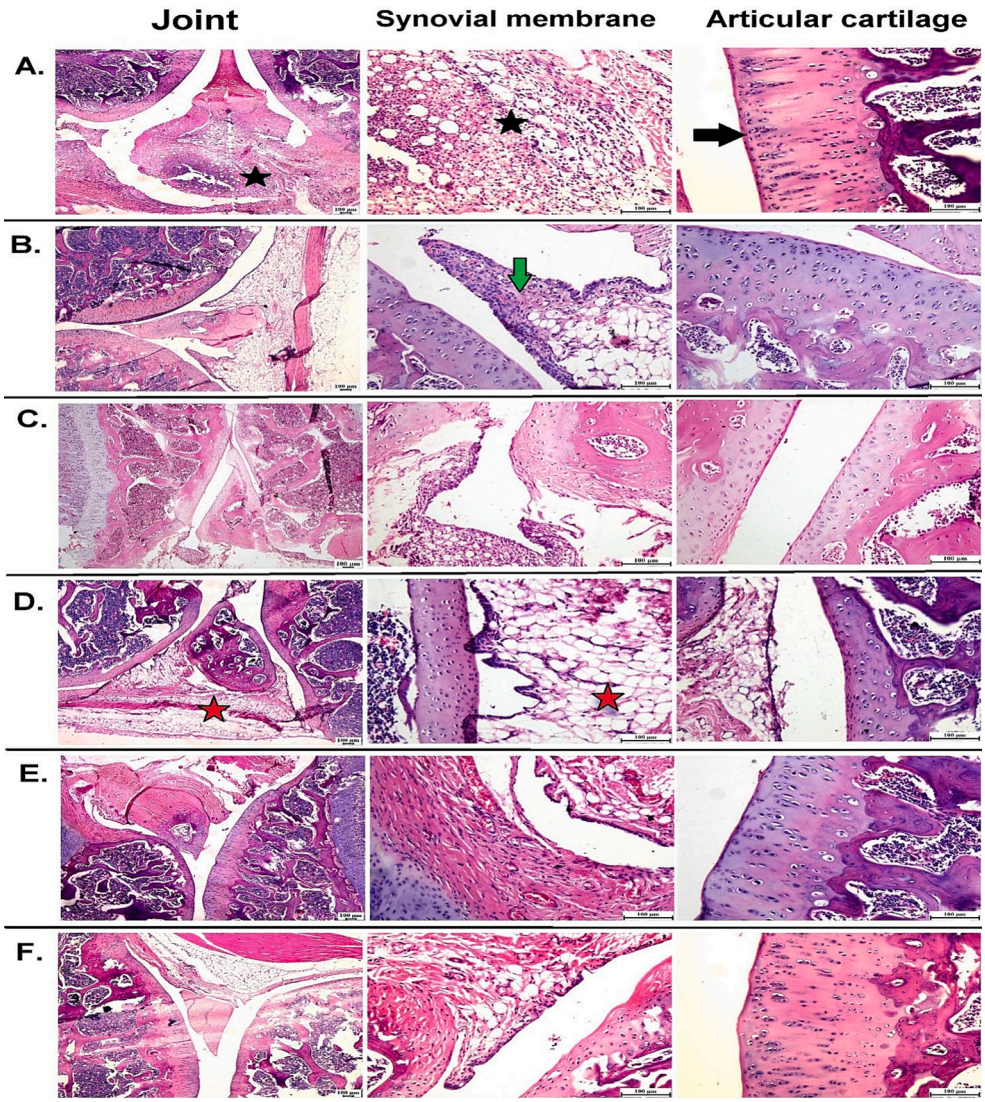

Fig. 7. Photomicrographs of joints (H&E). (A) positive control group, showing marked inflammatory cells infiltration extending into the joint capsule (black stars) and some degenerating chondrocytes in the articular cartilage (black arrow), (B) HYP ointment group showing inflammation extending into the synovial membrane (green arrow) with periarticular edema. (C) HYP microneedles group showing moderate inflammation of the synovial membrane. (D) HYP EMLS microneedles group showing mild edema (red stars). (E) HYP EMLS microneedles (light) group showing apparently normal structure of the joint. (F) negative control group, showing a normal structure of the joint. (For interpretation of the references to colour in this figure legend, the reader is referred to the web version of this article.)

apparently normal. Normal structure of joint was noticed in negative control group.

Arthritis lesion scores were conducted in different experimental groups. The positive control group showed a significant increase in comparison with all experimental groups. A marked significant decrease was determined in the groups treated with HYP EMLS microneedles and HYP EMLS microneedles (light) when compared to other treated groups (Fig. 8).

Toluidine blue stained sections (Fig. 9) demonstrated lightly stained thin articular cartilage in positive control group. All treated group showed improvement in cartilage staining as HYP ointment and HYP microneedles groups showed mild increase in staining intensity, moderate staining was detected in HYP EMLS microneedles group and HYP EMLS microneedles (light) group showed apparently normal cartilage staining. Thick deeply stained articular surfaces were noticed in the negative control group.

These results implied that combining the photoactive HYP EMLs with Ho-MNs could alleviate the damage of RA induced in the cartilage area and even potentiate its recovery. And also revealed the superior effect of HYP EMLs even in absence of light over HYP solution injected using Ho-MNs.

To sum up, histopathological analysis results are long with joint diameter and ELISA. Even though in our experiment HYP ointment was applied daily for 14 days and HYP solution in microneedles and HYP EMLs in Ho-MNs were applied twice at 7-day intervals. Groups treated with HYP EMLs in Ho-MNs demonstrated superior joint healing compared to the HYP ointment group and HYP microneedles group. This may be attributed to the effect of nanoencapsulation on increasing the solubility of hydrophobic drugs especially since HYP was found to exist in the form of monomers in lipids (Abd-El-Azim et al., 2022; Zewail et al., 2021; Ho et al., 2009). The superior effect of HYP EMLs in microneedles over HYP ointment group clearly demonstrated the role of AdminPen™ Ho-MNs for intradermal injection of the nanoformulations where Ho-MNs succeeded in deeply depositing the developed HYP EMLs into the deeper layers of the skin to be further distributed into the arthritic joint.

It is worth mentioning that the superiority of the group treated with HYP EMLs in Ho-MNs in the presence of light over the group treated with HYP EMLs in the absence of light could be attributed to the effect of light on enhancing the activity of HYP and hence potentiating its

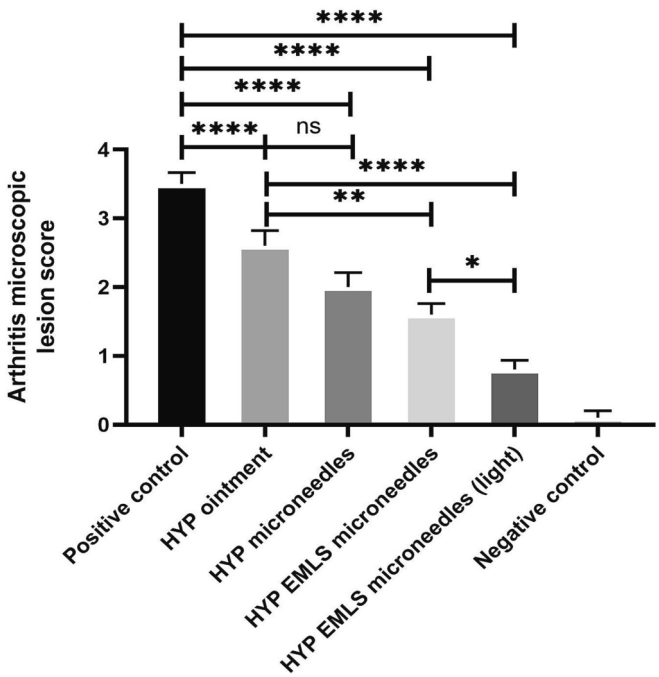

Fig. 8. Arthritis microscopic lesion score in different group. Values expressed as means ± SEM. Significant difference is conducted at $P < 0.05$.

pharmacological effects. This was in agreement with previous results reported that HYP activity increased significantly upon irradiation at its excitation wavelength (Gallardo-Villagrán et al., 2019; Abd-El-Azim et al., 2022; Barras et al., 2018). Besides, Karioti and Bilia (Karioti and Bilia, 2010) previously deduced that light application is essential for HYP to release ROS and induce its action.

In RA management, photosensitizers were proven to significantly decrease the levels of TNFα and IL1 (Yang et al., 2021). Considering HYP, specifically, earlier studies revealed the efficiency of photoactivated HYP (0–4 μM) in potentiating intracellular ROS production to induce mitochondrial apoptosis and significant death of human RA synovial (MH7A) cells. Mechanistically, irradiated HYP triggered morphological alterations in MH7A cells including cytoplasmic vacuolation and shrinking initiating the caspase cascade pathway and inhibiting NF-κB that eventually led to cell apoptosis (Zhang et al., 2018; Wang et al., 2022). Collectively, this study unveils new insights for developing the next generation of RA therapeutics through merging nanotechnology, PDT and MNs.

4. Conclusion

This work innovatively utilized AdminPen™ Ho-MNs for the non-invasive transdermal delivery of EMLs loaded with the photosensitizer, HYP, as a promising localized treatment modality of RA. HYP EMLs featured excellent characteristics regarding morphology, particle size, zeta potential and entrapment efficiency. Furthermore, AdminPen™ Ho-MNs allowed for precise, continuous and controlled delivery of HYP EMLs reaching the underlying layers of the skin where they could be rapidly distributed into the arthritic joint in high localized concentration. Additionally, in a rat model, treatment with irradiated HYP EMLs using Ho-MNs demonstrated nearly normal joint shape and diameter, superior joint healing, decreased levels of TNFα, IL1, HO and MMP 9, almost normal NRF2 level, apparently normal cartilage staining indicating for alleviated inflammation and potentiated recovery.

Strikingly, the presented novel combination of the photosensitive HYP EMLs and Ho-MNs showed a strong potential to target specific areas of inflammation in RA, reducing the risk of adverse side effects associated with systemic administration. Besides, it holds great promise in improving patient compliance, reducing needle phobia, minimizing the frequency of PDT dosage, and enhancing the efficacy of various therapeutics, making it a potential milestone in the medical field of arthritic diseases.

CRediT authorship contribution statement

Heba Abd-El-Azim: Investigation, Methodology, Writing – original

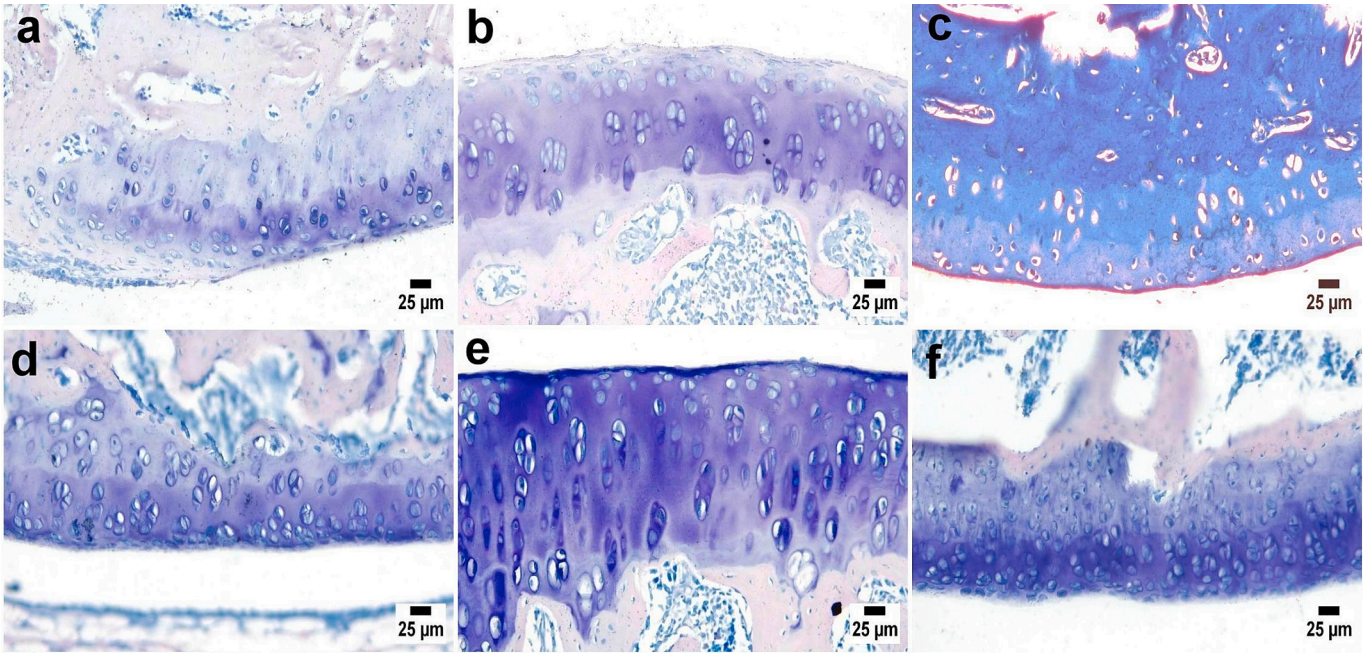

Fig. 9. Photomicrograph of joint (Toluidine blue), (a) positive control group showing lightly stained articular cartilage, (b) HYP ointment group showing mild stained cartilage, (c) and (d) HYP microneedles and HYP EMLS microneedles groups showing darker cartilage attaining and (e) HYP EMLS microneedles (light) group showing apparently normal cartilage and (f) negative control group showing dark stained cartilage. (For interpretation of the references to colour in this figure legend, the reader is referred to the web version of this article.)

draft. **Haidy Abbas:** Investigation, Methodology, Supervision, Validation. **Nesrine El Sayed:** Investigation, Methodology, Project administration. **Mohamed R. Mousa:** Data curation, Formal analysis, Methodology, Resources. **Hadil M. Elbardisy:** Data curation, Formal analysis, Investigation, Methodology. **Mariam Zewail:** Conceptualization, Data curation, Methodology, Writing – original draft, Writing – review & editing.

Declaration of competing interest

The authors declare that they have no known competing financial interests or personal relationships that could have appeared to influence the work reported in this paper.

Data availability

The authors do not have permission to share data.

References

Abbas, H., et al., 2021. Superparamagnetic iron oxide loaded chitosan coated bilosomes for magnetic nose to brain targeting of resveratrol. Int. J. Pharm. 610, 121244.
Abbas, H., et al., 2022a. Development and optimization of curcumin analog nanobilosomes using 21.31 full factorial design for anti-tumor profiles improvement in human hepatocellular carcinoma: in-vitro evaluation, in-vivo safety assay. Drug Deliv. 29 (1), 714–727.
Abbas, H., et al., 2022b. Development and evaluation of novel leflunomide SPION bioemulsomes for the intra-articular treatment of arthritis. Pharmaceutics 14 (10), 2005.
Abbas, H., El-Deeb, N.M., Zewail, M., 2021. PLA-coated Imwitor® 900 K-based herbal colloidal carriers as novel candidates for the intra-articular treatment of arthritis. Pharm. Dev. Technol. 26 (6), 682–692.
Abd-El-Azim, H., et al., 2022. Hollow microneedle assisted intradermal delivery of hypericin lipid nanocapsules with light enabled photodynamic therapy against skin cancer. J. Control. Release 849–869.
Abd-El-Azim, H., et al., 2022. Hollow microneedle assisted intradermal delivery of hypericin lipid nanocapsules with light enabled photodynamic therapy against skin cancer. J. Control. Release 348, 849–869.
Aggarwal, B.B., Harikumar, K.B., 2009. Potential therapeutic effects of curcumin, the anti-inflammatory agent, against neurodegenerative, cardiovascular, pulmonary, metabolic, autoimmune and neoplastic diseases. Int. J. Biochem. Cell Biol. 41 (1), 40–59.
Ahmed, S., Kassem, M.A., Sayed, S., 2020. Bilosomes as promising nanovesicular carriers for improved transdermal delivery: construction, in vitro optimization, ex vivo permeation and in vivo evaluation. Int. J. Nanomed. 15, 9783.
Anita, C., et al., 2021. Topical nanocarriers for management of rheumatoid arthritis: a review. Biomed. Pharmacother. 141, 111880.
Arya, J., Prausnitz, M.R., 2016. Microneedle patches for vaccination in developing countries. J. Control. Release 240, 135–141.
Balata, G.F., et al., 2020. Preparation and characterization of ivabradine HCl transfersomes for enhanced transdermal delivery. J. Drug Delivery Sci. Technol. 60, 101921.
Bancroft, J.D., Gamble, M., *Theory and Practice of Histological Techniques*. 2008: Elsevier Health Sciences.
Barras, A., et al., 2013. Hypericin-loaded lipid nanocapsules for photodynamic cancer therapy in vitro. Nanoscale 5 (21), 10562–10572.
Barras, A., et al., 2018. Improved photodynamic effect through encapsulation of two photosensitizers in lipid nanocapsules. J. Mater. Chem. B 6 (37), 5949–5963.
Bernal, C., et al., 2015. Photodynamic efficiency of hypericin compared with chlorin and hematoporphyrin derivatives in HEp-2 and Vero epithelial cell lines. Photodiagn. Photodyn. Ther. 12 (2), 176–185.
Boiy, A., et al., 2007. Effect of vehicles and esterification on the penetration and distribution of hypericin in the skin of hairless mice. Photodiagn. Photodyn. Ther. 4 (2), 130–139.
Bolat, Z.B., et al., 2020. Curcumin-and piperine-loaded emulsomes as combinational treatment approach enhance the anticancer activity of curcumin on HCT116 colorectal cancer model. Front. Bioeng. Biotechnol. 8, 50.
Borghi-Pangoni, F.B., et al., 2017. Preparation and characterization of bioadhesive system containing hypericin for local photodynamic therapy. Photodiagn. Photodyn. Ther. 19, 284–297.
Boskabady, M.H., et al., 2011. Pharmacological effects of Rosa damascena. Iran. J. Basic Med. Sci. 14 (4), 295.
Bushra, F., *Delivery of Denosumab via Hollow Microneedle*. 2020, Brac University.
Butler, S.H., et al., 1992. A limited arthritic model for chronic pain studies in the rat. Pain 48 (1), 73–81.
Chadha, S., et al., 2020a. Role of Nrf2 in rheumatoid arthritis. Curr. Res. Transl. Med.
Chadha, S., et al., 2020b. Role of Nrf2 in rheumatoid arthritis. Curr. Res. Transl. Med. 68 (4), 171–181.
Dragicevic-Curic, N., et al., 2010. Surface charged temoporfin-loaded flexible vesicles: in vitro skin penetration studies and stability. Int. J. Pharm. 384 (1–2), 100–108.
El-Nabarawi, M.A., et al., 2020. Bilosomes as a novel carrier for the cutaneous delivery for dapsone as a potential treatment of acne: preparation, characterization and in vivo skin deposition assay. J. Liposome Res. 30 (1), 1–11.
El-Shiekh, R.A., et al., 2021. Anti-inflammatory activity of Jasminum grandiflorum L. subsp. floribundum (Oleaceae) in inflammatory bowel disease and arthritis models. Biomed. Pharmacother. 140, 111770.
Farrugia, M., Baron, B., 2016. The role of TNF-α in rheumatoid arthritis: a focus on regulatory T cells. J. Clin. Transl. Res. 2 (3), 84.
Feng, X., et al., 2019. Immunomodulatory nanosystems. Adv. Sci. 6 (17), 1900101.
Fernandes, R.M.S.N., Silva, N.P.d., Sato, E.I., 2012. Increased myeloperoxidase plasma levels in rheumatoid arthritis. Rheumatol. Int. 32 (6), 1605–1609.
Firestein, G.S., 2003. Evolving concepts of rheumatoid arthritis. Nature 423 (6937), 356–361.
Gallardo-Villagrán, M., et al., 2019. Photosensitizers used in the photodynamic therapy of rheumatoid arthritis. Int. J. Mol. Sci. 20 (13), 3339.
Gill, B., et al., 2014. Emulsomes: An emerging vesicular drug delivery system. Asian J. Pharm. (AJP) 6 (2).
Gupta, J., Felner, E.I., Prausnitz, M.R., 2009. Minimally invasive insulin delivery in subjects with type 1 diabetes using hollow microneedles. Diabetes Technol. Ther. 11 (6), 329–337.
Hendrich, C., et al., 2001. Experimental photodynamic laser therapy for rheumatoid arthritis using photosan-3, 5-ALA-induced PPIX and BPD verteporfin in an animal model. Lasers Musculoskeletal Syst. 69–74.
Ho, Y.-F., et al., 2009. Lipid-mediated preferential localization of hypericin in lipid membranes. Biochim. Biophys. Acta (BBA)-Biomembranes 1788 (6), 1287–1295.
Karioti, A., Bilia, A.R., 2010. Hypericins as potential leads for new therapeutics. Int. J. Mol. Sci. 11 (2), 562–594.
Kay, J., Calabrese, L., 2004. The role of interleukin-1 in the pathogenesis of rheumatoid arthritis. Rheumatology 43 (suppl_3) p. iii2-iii9.
Kumar, N., et al., 2010. Emerging role of vesicular carriers for therapy of visceral leishmaniasis: conventional versus novel. Crit. Rev.™ Therapeutic Drug Carrier Syst. 27 (6).
Kumar, R., Seth, N., 2013. Emulsomes: an emerging vesicular drug delivery system. J. Drug Delivery Therapeutics 3 (6), 133–142.
Larraneta, E., et al., 2016. Microneedle arrays as transdermal and intradermal drug delivery systems: materials science, manufacture and commercial development. Mater. Sci. Eng. R. Rep. 104, 1–32.
Li, S., et al., 2021. Nanomaterials manipulate macrophages for rheumatoid arthritis treatment. Front. Pharmacol. 12, 699245.
Lima, A.M., et al., 2013. Hypericin encapsulated in solid lipid nanoparticles: phototoxicity and photodynamic efficiency. J. Photochem. Photobiol. B Biol. 125, 146–154.
Liu, Y.-L., et al., 2009. Suppression of complete Freund's adjuvant-induced adjuvant arthritis by cobratoxin. Acta Pharmacol. Sin. 30 (2), 219–227.
Maiuolo, J., et al., 2021. Endothelial dysfunction and extra-articular neurological manifestations in Rheumatoid Arthritis. Biomolecules 11 (1), 81.
Mehanna, M.M., et al., 2020. Anticancer activity of thymoquinone cubic phase nanoparticles against human breast cancer: formulation, cytotoxicity and subcellular localization. Int. J. Nanomed. 15, 9557.
Nafee, N., et al., 2013. Antibiotic-free nanotherapeutics: Hypericin nanoparticles thereof for improved in vitro and in vivo antimicrobial photodynamic therapy and wound healing. Int. J. Pharm. 454 (1), 249–258.
Odobasic, D., et al., 2014. Endogenous myeloperoxidase is a mediator of joint inflammation and damage in experimental arthritis. Arthritis Rheumatol. 66 (4), 907–917.
Paliwal, R., et al., 2009. Effect of lipid core material on characteristics of solid lipid nanoparticles designed for oral lymphatic delivery. Nanomed. Nanotechnol. Biol. Med. 5 (2), 184–191.
Permana, A.D., et al., 2019. Solid lipid nanoparticle-based dissolving microneedles: A promising intradermal lymph targeting drug delivery system with potential for enhanced treatment of lymphatic filariasis. J. Control. Release 316, 34–52.
Priyanka, K., Sahu, P.L., Singh, S., 2018. Optimization of processing parameters for the development of Ficus religiosa L. extract loaded solid lipid nanoparticles using central composite design and evaluation of antidiabetic efficacy. J. Drug Delivery Sci. Technol. 43, 94–102.
Prosperi, D., et al., 2017. Drug nanocarriers to treat autoimmunity and chronic inflammatory diseases. Seminars in Immunology. Elsevier.
Prosperi, D., et al. *Drug nanocarriers to treat autoimmunity and chronic inflammatory diseases*, in: *Semin. Immunol.* 2017. Elsevier.
Rahman, H.S., et al., 2013. Zerumbone-loaded nanostructured lipid carriers: preparation, characterization, and antileukemic effect. Int. J. Nanomed. 8, 2769.
Rizk, S.A., et al., 2021. Novel bioemulsomes for baicalin oral lymphatic targeting: development, optimization and pharmacokinetics. Nanomedicine 16 (22), 1983–1998.
Shih, C.-M., et al., 2019. Hypericin induced malformation, mortality and hepatotoxicity during zebrafish development. Curr. Topics Nutraceutical Res. 17 (4).
Srivastava, S., et al., 2017. Treatment of rheumatoid arthritis by targeting macrophages through folic acid tailored superoxide dismutase and serratiopeptidase. J. Drug Deliv. Sci. Technol. 41, 431–435.
Ucisik, H., Sleytr, U.B., Schuster, B., 2015. Emulsomes meet S-layer proteins: an emerging targeted drug delivery system. Curr. Pharm. Biotechnol. 16 (4), 392–405.
van Eden, W., Wagenaar-Hilbers, J.P., Wauben, M.H., 1996. Adjuvant arthritis in the rat. Curr. Protocols Immunol. 19, p. 15.4. 1–15.4. 8.
Waghule, T., et al., 2019. Microneedles: a smart approach and increasing potential for transdermal drug delivery system. Biomed. Pharmacother. 109, 1249–1258.

Wang, X., et al., 2014. Optimization of extraction process of hypericin from St. John's Wort by central composite design-response surface methodology. J. Chem. Pharm. Res. 6 (7), 1667–1675.
Wang, X., et al., 2022. The role of reactive oxygen species in the rheumatoid arthritis-associated synovial microenvironment. Antioxidants 11 (6), 1153.
Wang, J., et al., 2022. Promising strategies for transdermal delivery of arthritis drugs: microneedle systems. Pharmaceutics 14 (8), 1736.
Wang, Q., Sun, X., 2017. Recent advances in nanomedicines for the treatment of rheumatoid arthritis. Biomater. Sci.
Weng, C., et al., 2021. Comparative efficacy and safety of Janus kinase inhibitors and biological disease-modifying antirheumatic drugs in rheumatoid arthritis: a systematic review and network meta-analysis. Therapeutic Adv. Musculoskeletal Dis. 13, p. 1759720X21999564.
Yang, M., et al., 2017. Nanotherapeutics relieve rheumatoid arthritis. J. Control. Release 252 (Supplement C), 108–124.
Yang, D., et al., 2021. Application of photodynamic therapy in immune-related diseases. Photodiagn. Photodyn. Ther. 34, 102318.
Youssef, T., et al., 2012. Evaluation of hypericin-loaded solid lipid nanoparticles: Physicochemical properties, photostability and phototoxicity. Pharm. Dev. Technol. 17 (2), 177–186.
Yuan, F., et al., 2012. Development of macromolecular prodrug for rheumatoid arthritis. Adv. Drug. Deliv. Rev. 64 (12), 1205–1219.
Yuzhakov, V.V., 2010. The AdminPen™ microneedle device for painless & convenient drug delivery. Drug Deliv. Technol. 10 (4), 32–36.
Yuzhakov, V.V., *Microneedle array, patch, and applicator for transdermal drug delivery*. 2010, Google Patents.
Zewail, M., et al., 2019. Coated nanostructured lipid carriers targeting the joints–an effective and safe approach for the oral management of rheumatoid arthritis. Int. J. Pharm. 567, 118447.
Zewail, M., et al., 2021. Synergistic and receptor-mediated targeting of arthritic joints via intra-articular injectable smart hydrogels containing leflunomide-loaded lipid nanocarriers. Drug Deliv. Transl. Res. 11 (6), 2496–2519.
Zewail, M., 2021. Folic acid decorated chitosan-coated solid lipid nanoparticles for the oral treatment of rheumatoid arthritis. Ther. Deliv. 12 (4), 297–310.
Zewail, M., et al., 2022. Hyaluronic acid coated teriflunomide (A771726) loaded lipid carriers for the oral management of rheumatoid arthritis. Int. J. Pharm. 623, 121939.
Zewail, M., et al., 2022. Lipidic cubic-phase leflunomide nanoparticles (cubosomes) as a potential tool for breast cancer management. Drug Deliv. 29 (1), 1663–1674.
Zewail, M., Nafee, N., Boraie, N., 2021. Intra-articular dual drug delivery for synergistic rheumatoid arthritis treatment. J. Pharm. Sci. 110 (7), 2808–2822.
Zhang, K., et al., 2018. Hypericin-photodynamic therapy inhibits proliferation and induces apoptosis in human rheumatoid arthritis fibroblast-like synoviocytes cell line MH7A. Iran. J. Basic Med. Sci. 21 (2), 130.
Zhang, Y., et al., 2022. Transdermal delivery of inflammatory factors regulated drugs for rheumatoid arthritis. Drug Deliv. 29 (1), 1934–1950.
Zhang, W., et al., 2022. Recent advances of microneedles and their application in disease treatment. Int. J. Mol. Sci. 23 (5), 2401.
Zhou, X., Chen, Z., 2015. Preparation and performance evaluation of emulsomes as a drug delivery system for silybin. Arch. Pharm. Res. 38 (12), 2193–2200.